Adsorption of Rh(III) complexes from chloride solutions obtained by leaching chlorinated spent automotive catalysts on ion-exchange resin Diaion WA21J

Shaobo Shen [a,b,*], Tonglin Pan [a], Xinqiang Liu [a], Lei Yuan [a], Jinchao Wang [a,b], Yongjian Zhang [a], Zhanchen Guo [a]

[a] *Key Laboratory of Ecological and Recycling Metallurgy, Ministry of Education of China, Beijing 100083, China*
[b] *Department of Physical Chemistry, School of Metallurgical and Ecological Engineering, University of Science and Technology Beijing, Beijing 100083, China*

ARTICLE INFO

ABSTRACT

It was found that Rh, Pd and Pt contained in the spent ceramic automotive catalysts could be effectively extracted by dry chlorination with chlorine. In order to concentrate Rh(III) ions contained in the chloride solutions obtained, thermodynamic and kinetics studies for adsorption of Rh(III) complexes from the chloride solutions on an anionic exchange resin Diaion WA21J were carried out. Rh, Pd, Pt, Al, Fe, Si, Zn and Pb from the chloride solution could be adsorbed on the resin. The distribution coefficients (K_d) of Rh(III) decreased with the increase in initial Rh(III) concentration or in adsorption temperature. The isothermal adsorption of Rh(III) was found to fit Langmuir, Freundlich and Dubinin–Kaganer–Radushkevich models under the adsorption conditions. The maximum monolayer adsorption capacities Q_{max} based on Langmuir adsorption isotherms were 6.39, 6.61 and 5.81 mg/g for temperatures 18, 28 and 40 °C, respectively. The apparent adsorption energy of Rh was about −7.6 kJ/mol and thus Rh(III) adsorption was a physical type. The experimental data obtained could be better simulated by pseudo-first-order kinetic model and the activation energy obtained was 6.54 J/mol. The adsorption rate of Rh(III) was controlled by intraparticle diffusion in most of time of adsorption process.

© 2010 Elsevier B.V. All rights reserved.

1. Introduction

The monolithic automotive catalysts are typically cordierite type honeycombs with platinum, palladium and rhodium. These catalysts are called 'three-way' catalysts, since they not only oxidize carbon monoxide and hydrocarbons but also reduce various nitrous oxides. The average loading of platinum group metals (PGMs) per catalytic converter has been 0.05 troy ounces of platinum, 0.02 troy ounces of palladium and 0.005 troy ounces of rhodium [1]. About 34% of total platinum, 55% of total palladium and 95% of total rhodium demand is now used for the production of automotive catalysts [2]. Each year, approximately 10 million automobiles are scrapped in the United States. Based on an equivalent number of converters, it is estimated that 500,000 troy ounces of platinum and 200,000 troy ounces of palladium and 50,000 troy ounces of rhodium will be wasted annually just in the United States [1]. The annual world consumption of these metals for auto-catalyst use could double or triple the above numbers [1]. Since these metals are in limited supply, a successful process for their recovery

from catalytic converters will play an important part in their future availability and prices. For such PGM recovery processes to be cost-effective, well over 90% of these precious metals must be recovered [2].

In the 20 year than since 1975, although more than 568,000 kg of PGMs have been used in automotive catalysts in the USA alone, only 10% of them have been recovered [3]. Dissolution of palladium, platinum and rhodium presents special problems owing to their generally high ionization potential (the first ionization potential of Pd = 8.3 eV, Pt = 9.0 eV and Rh = 7.5 eV). This coupled with the complex variety of elements in the used catalytic converter makes it difficult to leach these metals from the catalyst, and to isolate them from the pregnant solution. Less than 45% and 60% of Rh and Pt, respectively, from spent auto-catalysts were recovered by dissolving the auto-catalysts by using aqua-regia at 95 °C [2].

There is a range of hydrometallurgical or pyrometallurgical processes used in PGM recovery. The pyrometallurgical processes usually involved the melting of crushed auto-catalyst and flux materials in a crucible containing a molten collector metal such as iron or copper at high temperatures, using a plasma torch [3]. The resulting molten slag is allowed to settle for a period of time while the PGM is recovered into the collector metal at the base of the crucible. After that aqua-regia is usually used to dissolve PGMs in the metal collector phase. Long settling time was required for the separation of slag and metal collector. Moreover,

---

operating temperatures for this method were in the range 1500–1650 °C in order to melt cordierite support. The main problems related to pyrometallurgical method are that many steps are involved and the consumptions are high in energy and materials.

Dry chlorination methods for extracting PGMs from auto-catalysts were developed in recent years [2,4–6]. In the methods, the powder of crushed spent auto-catalyst containing PGMs were usually first calcined and then chlorinated at 500–800 °C with chlorine in the presence of reducing agent such as carbon monoxide [2]. After that a diluted hydrochloric acid was used to leach PGMs from the chlorinated powder of spent auto-catalyst. Finally, a chloride solution containing Rh, Pd and Pt was obtained as filtrate by separating solids residue by filtration. The extraction efficiencies of Pd, Pt and Rh of dry chlorination methods were usually higher than other methods, especially for Rh [4]. The cordierite material, which was the support of auto-catalyst, was almost not attacked by chlorine under the experimental conditions. This resulted in a less consumption in chlorine.
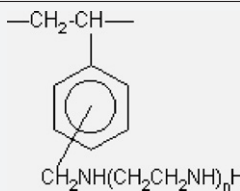
Solvent extraction has been widely used for separation of PGMs from aqueous solutions [7,8]. The prerequisite for this process is that the concentration of each PGM in aqueous solution must be over several hundreds of ppm. However, the concentrations of Rh in the chloride solution obtained by leaching chlorinated spent automotive catalysts were usually less than 100 ppm. Therefore, a pre-concentration of Rh(III) in the chloride solution was required. Adsorbing Rh in the chloride solution with ionic exchange resins is a possible way to concentrate Rh in the chloride solution. If PGM in the chloride solution could be adsorbed efficiently, Rh would be enriched by eluting them from the adsorbed resin or transforming the adsorbed resin into ash by ashing. It was found in this work that weakly basic anionic exchange resin Diaion WA21J (Mitsubishi Chemical Company) could selectively adsorb low concentrations of Pd, Pt and Rh simultaneously from the chloride solutions. Therefore, adsorption of Rh(III) complexes from the chloride solutions with resin Diaion WA21J was studied in this work. Besides Pd, Pt and Rh, the chloride solutions also contained Al, Mn, Fe, Mg, Si, Ni, Zn and Pb, etc. The presence of these co-existent ions probably interfered in the adsorption of Rh(III) ions on the resin Diaion WA21J. The HCl concentration in the chloride solution used in this work was about 10% (w/w). So far nothing has been mentioned in the literature concerning adsorbing Rh(III) ions with ion-exchange resins from such kind of chloride solutions. Thus thermodynamic and kinetics studies for adsorption of Rh(III) ions from the chloride solutions on anionic exchange resin Diaion WA21J was conducted in this work.

2. Materials and methods

2.1. Chloride solution

The chloride solutions were obtained by leaching the chlorinated powder of crushed spent auto-catalyst containing PGMs according to the literatures [2,4]. The powder of crushed ceramic auto-catalyst was first burnt in air at 800 °C and then chlorinated with $Cl_2 + CO$ at 650 °C. The chlorinated powder was then leached with 10% (w/w) HCl. Finally, a chloride solution containing Pd, Rh and Pt was obtained as filtrate by separating the solid residue by filtration. The chloride solutions thus obtained were used in the adsorption experiments of this work without any adjustment in solution pH before use. The concentrations of Rh from the chloride solution were analyzed by ICP-MS (Thermofisher XII, USA) and the concentrations of the other elements from the chloride solution were analyzed by ICP-AES (J.Y. ULTIMA, France). The concentrations of all main elements from the filtrate, which are denoted as initial concentrations, are listed in Table 1.

2.2. Ion-exchange resin Diaion WA21J

The commercial ion-exchange resin Diaion WA21J from Mitsubishi Chemical Company was used in this work. It is a weakly basic anionic exchanger with the functional group ($-CH_2N(CH_2CH_2NH)_nH$) and a polystyrene skeleton. Its properties are listed in Table 2.

2.3. Methods used

The extracted chloride solution containing 10% HCl was used directly in the adsorption experiments without any adjustment in solution pH. Batch technique was selected to obtain equilibrium and kinetic data.

The amount of Rh(III) ions adsorbed onto anion exchangers, Q_t, was calculated by Eq. (1):

$$Q_t = \frac{(C_0 V_0 - C_t V_t)}{W} \times 0.001 \tag{1}$$

where C_0 and C_t are the concentrations of Rh ions at initial and after time t in the aqueous phase (mg/L), respectively; V_0 is the initial volume of the chloride solution containing Rh ions (mL); V_t is the filtrate volume (mL); W is the weight of the original ion-exchange resin (g).

Table 2
Properties of ion-exchange resin Diaion WA21J.

Properties	Quantitative value	
Chemical structure	—CH₂-CH— (polystyrene ring) CH₂NH(CH₂CH₂NH)ₙH	
Ion-exchange capacity (meq/mL)	>2.0	
Water content (%)	40–52	
Particle size distribution>1180 μm<300 μm	<5%	<1%
Effective size (mm)	>0.40	
Maximum temperature (°C)	<100	

Table 1
Element concentrations (in ppm) in the chloride solution before and after adsorption (chloride solution = 300 mL; resin = 10.000 g; 21 °C; 150 rpm; 40 h).

Ions	Pd	Pt	Rh	Al	Mn	Fe	Mg	Si
Initial concentration	43.9	29.5	8.9	999.8	736.3	560.0	391.9	312.9
Concentration after adsorption	4.3	2.5	0.9	992.9	743.5	556.5	400.3	281.7
Adsorption efficiency (%)	90.21	91.53	89.89	0.69	−0.98	0.63	−2.14	9.98

Ions	Ca	Zn	Cr	Pb	Cu	La	Ba	Ni
Initial concentration	221.3	242.0	53.9	42.8	20.4	13.1	2.3	377.0
Concentration after adsorption	227.4	199.5	55.2	19.2	20.5	13.3	2.3	385.0
Adsorption efficiency (%)	−2.76	17.58	−2.41	55.14	−0.49	−1.53	0.00	−2.12

The distribution coefficient of Rh(III), K_d (L solution/kg resin), is defined as the ratio of the Rh(III) concentration in the solid resin (C_1) to that in the solution (C_2) and calculated by the Eq. (2):

$$K_d = \frac{C_1}{C_2} \times 10^3 \qquad (2)$$

where C_1 is the Rh(III) mass (in mg) adsorbed in one gram of solid resin (mg/g); C_2 is the Rh(III) mass (mg) left in one liter of chloride solution after adsorption (mg/L).

2.3.1. Adsorption kinetics

Sixty milliliter of chloride solution of same Rh(III) concentration and 0.5000 g of resin Diaion WA21J were placed in each of eleven glass bottles of 200 mL with tight screwed plastic lid. Then the bottles were put in an incubator (BS-1E, China) agitated at 150 rpm and controlled at a preset temperature with a variation of ±1 °C. At preset intervals of time (0.5–40 h), one of solutions was taken out of the incubator each time and filtrated immediately on Whatman GF-A membrane. The filtrates thus obtained were analyzed for Rh(III) concentration.

2.3.2. Adsorption isotherm

Sixty milliliter of chloride solution of different Rh(III) concentrations were placed in each of 12 glass bottles with tight screwed plastic lid. Then 0.1000 g of resin Diaion WA21J was placed in each of bottle at an interval of 1 h. After that each bottle was put in an incubator (BS-1E, China) agitated at 150 rpm and controlled at a preset temperature with a variation of ±1 °C. After 40 h, one of the solutions was taken out of the incubator each time and filtrated immediately on Whatman GF-A membrane. The filtrates thus obtained were analyzed for Rh(III) concentration.

2.3.3. Nitrogen adsorption/desorption measurements

The experiments of nitrogen adsorption and desorption were conducted to measure BET specific surface area, average pore diameter and total pore volume of resins by using Quantachrome Autosorb-1. Two resins were employed in the measurement. One was original Diaion WA21J resin. The other was a used Diaion WA21J resin, which was obtained by using the following treatment. A 300 mL of the chloride solution was placed in one glass bottle with plastic lid. Then 1.0000 g of resin Diaion WA21J was placed in the glass bottle. After that the bottle was put in an incubator (BS-1E, China) agitated at 150 rpm and controlled at 18 °C for 40 h. Then the glass bottle was taken out of the incubator and filtrated immediately on Whatman GF-A membrane. The solid resin left on the filter membrane after filtration was dried at 30 °C for 12 h. After that the dried resin was used in nitrogen adsorption/desorption measurements.

3. Results and discussion

3.1. Metals adsorption on the resin

In addition to PGMs (Pd, Pt and Rh), there were also about 13 metal ions which were present in the chloride solution. The preliminary investigation of their adsorption on the resin Diaion WA21J was carried out. The chloride solution of 300 mL was contacted with 10.0000 g of the resin for 40 h. After that, the sample was filtered on Whatman GF-A membrane without any washing and the filtrate was used for chemical analysis. The results are listed in Table 1. The adsorption efficiencies of metals could be simply expressed by the percentage of metal concentration variation if the volume variation of the chloride solutions before and after adsorption was negligible. The adsorption efficiencies of Rh, Pd, Pt, Al, Fe, Si, Zn and Pb were 89.89%, 90.21%, 91.53%, 0.69%, 0.63%, 9.98%, 17.58% and
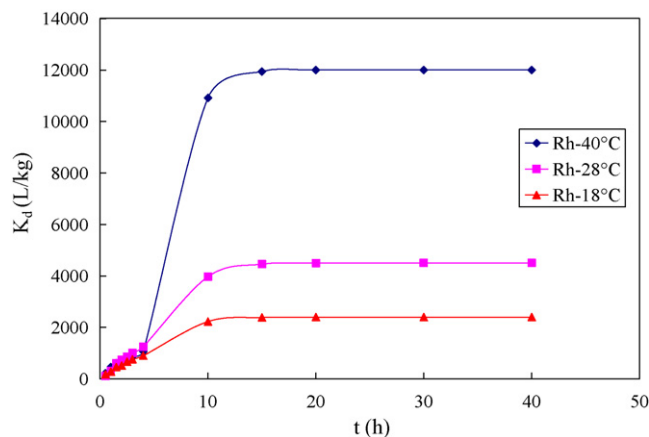

Fig. 1. Variation of distribution coefficient K_d of Rh(III) with time at different temperatures (chloride solution = 60 mL; resin = 0.5000 g; 150 rpm).

55.14%, respectively, and the adsorptions of Mn, Ca, Mg, Ni, Cu, La and Ba on the resin were negligible (Table 1).

3.2. Effect of the contact time

The distribution coefficients (K_d) of Rh(III) reached plateaus about for 10 h at 18, 28 and 40 °C (Fig. 1). It implies that the adsorption equilibrium times for Rh(III) from the chloride extract was about 10 h at 18, 28 and 40 °C. Based on these findings and the adsorption equilibrium times for Pt and Pd, an agitation time of 40 h was used in all thermodynamic experiments to make sure the adsorption equilibrium were sufficiently reached for Rh, Pt and Pd.

3.3. Thermodynamic studies of Rh(III) adsorption

It is important to evaluate the most appropriate correlations for equilibrium data, to optimize the design of an adsorption system. Freundlich, Langmuir, Dubinin–Kaganer–Radushkevich isotherm models were used to describe the adsorption equilibrium. Isothermal experimental data were obtained at an equilibrium time of 40 h for different initial concentrations of Rh(III) ion in the chloride solutions.

3.3.1. Effect of initial concentration of Rh(III) on distribution coefficient

The distribution coefficients (K_d) of Rh(III) for three temperatures (18, 28 and 40 °C) decreased with the increase in initial Rh(III) concentration or in temperature (Fig. 2).

3.3.2. Freundlich adsorption isotherm

The empirical Freundlich equation is based on adsorption on a heterogeneous surface and derived from the assumption that the adsorption sites are distributed exponentially with respect to the heat of adsorption [9,10]. The logarithmic linear form of Freundlich equation is given below by Eq. (3).

$$\ln Q_{eq} = \ln K_F + \frac{1}{n} \ln C_{eq} \qquad (3)$$

where Q_{eq} (mg/g) and C_{eq} (mg/L) are the amount of adsorbed Rh(III) per unit weight of adsorbent and unabsorbed Rh(III) concentration in solution at equilibrium, respectively, and K_F and $1/n$ the Freundlich constants representing the adsorption capacity (mg$^{1-1/n}$ g^{-1} L$^{1/n}$) and intensity (dimensionless) of the adsorbent, respectively. The values of $1/n$ less than 1 represent a favorable adsorption [9].

The equilibrium data were fitted to Freundlich equation. The plot for this is shown in Fig. 3. The linear plots of ln Q_{eq} versus ln C_{eq}
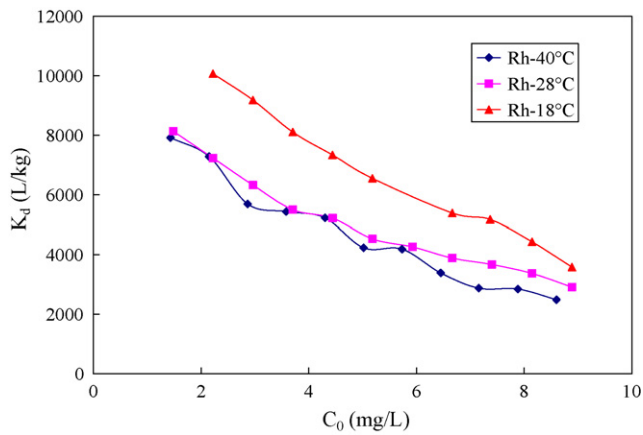
Fig. 2. Variation of distribution coefficient K_d of Rh(III) with initial concentration of Rh(III) at different temperatures (chloride solution = 60 mL; resin = 0.1000 g; 150 rpm; 40 h).
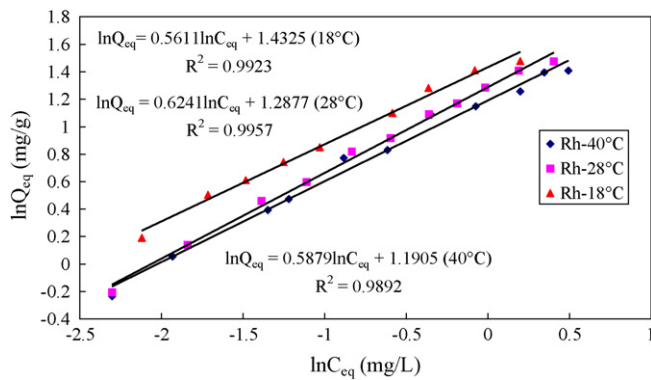

Fig. 3. Freundlich plot for adsorption of Rh(III) on resin Diaion WA21J at different temperatures (chloride solution = 60 mL; resin = 0.1000 g; 150 rpm; 40 h).
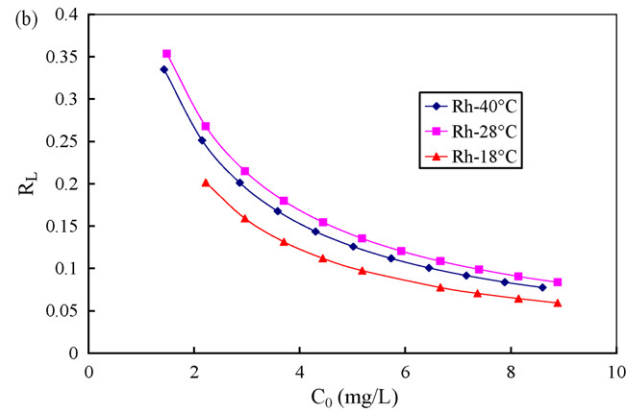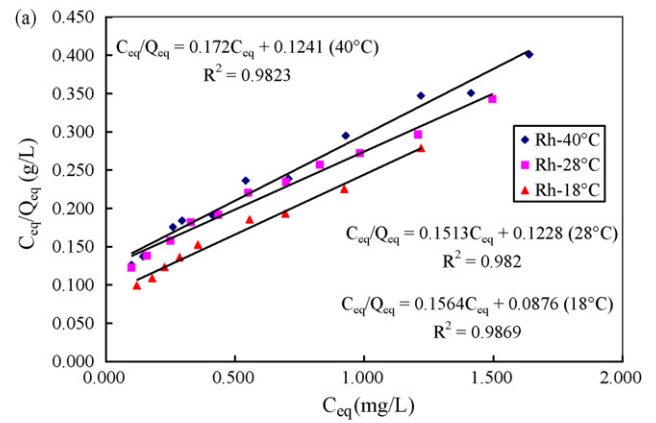

Fig. 4. (a) Langmuir plot for adsorption of Rh(III) on resin Diaion WA21J at different temperatures (b) Variation of equilibrium parameter R_L with initial concentration of Rh(III) at different temperatures (chloride solution = 60 mL; resin = 0.1000 g; 150 rpm; 40 h).

(Fig. 3) with regression correlation coefficients R^2 all greater than 0.98 indicated the applicability of Freundlich adsorption isotherm for the cases at three temperatures. The conformity between experimental data and the model predicted values was expressed by the regression correlation coefficient (R^2, values close or equal to 1). A relatively high R^2 value indicates that the model successfully describes the experimental data. The values of K_F and $1/n$ were calculated from the intercept and slope of the linear plots between $\ln Q_{eq}$ and $\ln C_{eq}$ and are shown in Table 3. The values of K_F were 4.19, 3.62 and 3.29 for the temperatures 18, 28 and 40 °C, respectively (Table 3). An increase in temperature resulted in a decrease in K_F indicating that the adsorption capacity of the resin for Rh(III)

decreased with the increase in temperature. This finding was also indirectly supported by the values of K_d in Fig. 2. The values of $1/n$ were 0.56, 0.62 and 0.59 for the temperatures 18, 28 and 40 °C, respectively (Table 3), which indicated that the Rh(III) adsorption on resin Diaion WA21J was favorable for the three temperatures.

3.3.3. Langmuir adsorption isotherm

The Langmuir adsorption isotherm is based on the assumption that all sites possess equal affinity for the adsorbate [9,10]. The Langmuir isotherm is expressed by Eq. (4).

$$\frac{C_{eq}}{Q_{eq}} = \frac{1}{bQ_{max}} + \frac{C_{eq}}{Q_{max}} \tag{4}$$

where b (L/mg) and Q_{max} (mg/g) are the Langmuir constant and the theoretical monolayer saturation capacity of the resin, respectively. High b values indicate high adsorption affinity.

The equilibrium data were fitted to Langmuir equation. The plot for this is shown in Fig. 4(a). The linear plots of C_{eq}/Q_{eq} versus C_{eq} (Fig. 4(a)) with regression correlation coefficients R^2 all greater than 0.98 indicated the applicability of Langmuir adsorption isotherm for the cases at three temperatures. The values of b and Q_{max} calculated from the intercept and slope of the linear plots are shown in Table 3. The values of Q_{max} were 6.39, 6.61 and 5.81 mg/g for the temperatures 18, 28 and 40 °C, respectively (Table 3). It indicated that saturation Rh(III) adsorption capacity Q_{max} reached a maximum at 28 °C. The values of b were 1.79, 1.23 and 1.39 for the temperatures 18, 28 and 40 °C, respectively (Table 3). The largest value of b at 28 °C also implied the strongest bonding of Rh(III) to the resin occurred at this temperature.

Table 3
Constants of adsorption isotherms of various models for Rh(III) on resin Diaion WA21J (chloride solution = 60 mL; resin = 0.1000 g; 150 rpm; 40 h).

Model	Parameter	Temperature (°C)		
		18	28	40
Freundlich	K_F (mg$^{1-1/n}$ g^{-1} L^n)	4.19	3.62	3.29
	$1/n$	0.5611	0.6241	0.5879
	R^2	0.9923	0.9957	0.9892
Langmuir	Q_{max} (mg/g)	6.39	6.61	5.81
	b (L/mg)	1.79	1.23	1.39
	R^2	0.9869	0.982	0.9823
DKR	X_m (mg/g)	12.15	12.00	10.46
	B (mol^2/kJ^2)	0.0086	0.009	0.0079
	E_{ad} (kJ/mol)	7.62	7.45	7.96
	R^2	0.9956	0.9985	0.9949

In order to predict the adsorption efficiency of the adsorption process, the dimensionless equilibrium parameter R_L was determined by using the following Eq. (5) [9,10]:

$$R_L = \frac{1}{1 + bC_0} \tag{5}$$

where C_0 is the initial concentration of Rh(III), and b the Langmuir constant (Eq. (4)). Values of $R_L < 1$ represent favorable adsorption and values greater than 1.0 represent unfavorable adsorption [9,10]. Also R_L values equal to 0 indicate irreversible adsorption. From our study, R_L values for Rh(III) ion adsorption ranged from 0.06 to 0.35 for the three temperatures (Fig. 4(b)). This is for initial concentration of 1.4–8.8 mg/L of Rh(III) ions. Therefore, the adsorption process is favorable for Rh(III). Moreover, R_L values decreased with the increase in initial Rh(III) concentration. A higher initial Rh(III) concentration was more favorable for the adsorption of Rh(III) on the resin. So the resin Diaion WA21J can be used as a potential source for adsorption of Rh(III) from the chloride solution.

There is a great difference between ion-exchange capacity (>2 mmol/g) of the resin (Table 2) and the adsorbed amount of Rh at equilibrium Q_{eq} at 18 °C (0.48 mg Rh/g resin or 0.0046 mmol Rh/g resin) (not shown). The value of Q_{max} at 18 °C calculated from Langmuir isotherm was also as low as 6.39 mg Rh/g resin (Table 3), which gives 0.062 mmol Rh/g resin. It is obvious that only small amount of adsorption sites were used for Rh adsorption. There are two possible explanations for this phenomenon. First, this work concerned the adsorption of Rh in the presence of Pd and Pt. It was found by us that Pd and Pt showed higher adsorption percentages on the resin than Rh did (Table 1). In addition, the ions of other metals such as Si, Zn, Pb, Al, and Fe were also adsorbed on the resin (Table 1). Probably most of adsorption sites on the resin were preferentially occupied by other metal ions other than Rh, which resulted in the low adsorption amount of Rh(III). Second, Pd and Pt ions in the chloride solution existed mainly in the forms of smaller molecules such as $PdCl_4^{2-}$ and $PtCl_6^{2-}$ than $Rh(H_2O)_2Cl_4^-$ under the present conditions (3.3 M HCl). Compared to the ions of Pd and Pt, it was more difficult for $Rh(H_2O)_2Cl_4^-$ to adsorb on the external surfaces or inside the pores of anionic exchange resin Diaion WA21J, considering $Rh(H_2O)_2Cl_4^-$ is a macro-molecule and has low negative valence state. Thus the adsorbed amount of Rh was much lower than the ion-exchange capacity of the resin. Upto now, few ion-exchange resins were found to have high adsorption capacity for Rh(III).

3.3.4. Dubinin–Kaganer–Radushkevick adsorption isotherm

Langmuir and Freundlich isotherms do not give any idea about adsorption mechanism. In order to distinguish between physical and chemical adsorption the data was subjected to the Dubinin–Kaganer–Radushkevich (DKR) isotherm model [11–13]. The DKR equation is expressed as:

$$\ln Q_{eq} = \ln X_m - B\varepsilon^2 \tag{6}$$

where ε (Polanyi potential) is $[RT(1+(1/C_{eq}))]$ (kJ/mol), C_{eq} the unabsorbed Rh(III) concentration in solution at equilibrium (mmol/L), X_m the Dubinin–Kaganer–Radushkevich constant related to the maximum Rh(III) adsorption capacity of the resin (mg/g), B the DRK constant related to the free energy of adsorption per mole of the adsorbate as it migrates to the surface of the adsorbent from infinite distance in the solution (mol²/kJ²). The plots of $\ln Q_{eq}$ versus ε^2 (Fig. 5) yielded straight lines with regression correlation coefficients R^2 all greater than 0.89, which indicated the applicability of DKR adsorption isotherm. The values of X_m and B were calculated from the intercept and slope of the linear plots are shown in Table 3. The values of X_m calculated from DKR adsorption isotherms were 12.15, 12.00 and 10.46 mg/g for the temperatures 18, 28 and 40 °C, respectively, which implied that the Rh(III) monolayer sat-
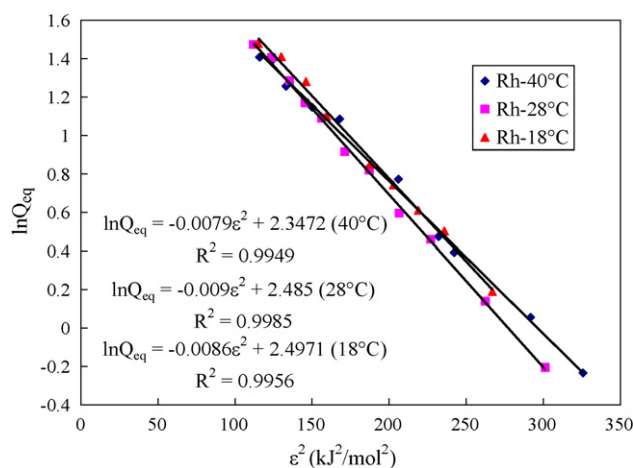

Fig. 5. DKR plot for adsorption of Rh(III) on resin Diaion WA21J at different temperatures (chloride solution = 60 mL; resin = 0.1000 g; 150 rpm; 40 h).

uration adsorption capacity (mg/g) on the resin decreased with the increase in temperature. This finding was agreement with that obtained from Langmuir adsorption isotherm (Table 3).
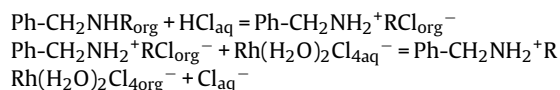
The apparent adsorption energies (E_{ad}) for PGM based on Dubinin–Kaganer–Radushkevich isotherm [11–13] were calculated using Eq. (7).

$$E_{ad} = \frac{-1}{\sqrt{2B}} \tag{7}$$

The calculated E_{ad} were −7.62, −7.45 and −7.96 kJ/mol for the temperatures 18, 28 and 40 °C, respectively (Table 3). It implied that the adsorption strengths of Rh(III) on the resin were almost the same at the three temperatures.

It is known that magnitude of apparent adsorption energy E_{ad} is useful for estimating the type of adsorption. If this value is below 8 kJ/mol the adsorption type can be explained by physical adsorption, between 8 and 16 kJ/mol the adsorption type can be explained by ion exchange, and over 16 kJ/mol the adsorption type can be explained by a stronger chemical adsorption than ion exchange [11–13]. The values of E_{ad} found in this study were between 7.62 and 7.76 kJ/mol (Table 3), which implied Rh(III) adsorption on the resin was basically a physical type, but close to an ion-exchange type.

The chloride solutions obtained from leaching chlorinated autocatalysts had high oxidation–reduction potential, therefore Rh(III) was the main valence state. Furthermore, in the chloride solution containing about 10% (w/w) HCl (or 3.3 M HCl), Rh(III) existed in the form of Rh(III) complex such as $Rh(H_2O)Cl_5^{2-}$ and $Rh(H_2O)_2Cl_4^-$. Thus the possible mechanism for the adsorption of Rh(III) complex on the resin Diaion WA21J (Ph-CH₂NHR) could be speculated as follows.

$$Ph\text{-}CH_2NHR_{org} + HCl_{aq} = Ph\text{-}CH_2NH_2{}^+RCl_{org}{}^-$$
$$Ph\text{-}CH_2NH_2{}^+RCl_{org}{}^- + Rh(H_2O)_2Cl_{4aq}{}^- = Ph\text{-}CH_2NH_2{}^+R$$
$$Rh(H_2O)_2Cl_{4org}{}^- + Cl_{aq}{}^-$$

where the subscripts 'aq' and 'org' denote species in the aqueous and resin phases, respectively.

3.4. Kinetic studies of Rh(III) adsorption

Kinetic adsorption experiments were carried out in this work to investigate the adsorption rate and adsorption mechanism of Rh(III). It is generally accepted that the adsorption includes the following processes (i) diffusion of the adsorbate from the bulk

Table 4
Kinetic parameters for the effect of temperatures on the adsorption of Rh(III).

	18 °C	28 °C	40 °C
Pseudo-first-order			
k_1 (h^{-1})	0.49	0.52	0.59
R^2	0.9996	0.9997	0.9996
Pseudo-second-order			
k_2 (g/mgh)	11.77	11.52	29.79
R^2	0.9705	0.9632	0.9803
Intraparticle diffusion (large pore diffusion)			
$k_{id,1}$ (mg/gh$^{-1/2}$)	0.13	0.18	0.10
c_1 (mg/g)	0.27	0.17	0.25
R^2	0.9984	0.9652	0.9639
Intraparticle diffusion (small pore diffusion)			
$k_{id,2}$ (mg/gh$^{-1/2}$)	0.03	0.04	0.02
c_2 (mg/g)	0.40	0.34	0.35
R^2	0.9086	0.9920	0.9910

solution to the liquid film surrounding the particle, (ii) diffusion of the adsorbate passing through the film to the particle surface (external diffusion or boundary layer diffusion), (iii) diffusion of the adsorbate from the surface to the internal sites (intraparticle diffusion or pore diffusion), and (iv) uptake of the adsorbate, which can involve several mechanisms: physicochemical adsorption, ion exchange, precipitation, or complexation. Bulk diffusion (i) is nonlimiting when agitation is sufficient to avoid concentration gradients in solution. The agitation rate of this work was 150 rpm. The last step, uptake (iv), is usually very rapid in comparison to the first three steps. Therefore, the overall rate of adsorption is probably controlled by the second or third step, whichever the diffusion resistance is larger, or a combination of both. The data obtained from the kinetic experiments were used to study the adsorption kinetics of Rh(III) ion from the chloride solution. The kinetics of Rh(III) adsorption on resin Diaion WA21J was analyzed using pseudo-first-order, pseudo-second-order, external diffusion and intraparticle diffusion models.

3.4.1. Pseudo-first-order and pseudo-second-order models

The pseudo-first-order rate expression based on solid capacity is generally expressed as follows [14]:

$$\frac{dQ_t}{dt} = k_1(Q_{eq} - Q_t), \tag{8}$$

$$\int_0^{Q_t} d\ln(Q_{eq} - Q_t) = -\int_0^t k_1 t, \tag{9}$$

$$\ln\left(1 - \frac{Q_t}{Q_{eq}}\right) = -k_1 t \tag{10}$$

The pseudo-second-order equation is also based on the adsorption capacity of the solid phase [14,15]. It is expressed as:

$$\frac{dQ_t}{dt} = k_2(Q_{eq} - Q_t)^2, \tag{11}$$

$$\int_0^{Q_t} d(Q_{eq} - Q_t)^{-1} = \int_0^t k_2 t, \tag{12}$$

$$\frac{1}{1 - (Q_t/Q_{eq})} = 1 + Q_{eq} k_2 t \tag{13}$$

where Q_{eq} and Q_t (both in mg/g) are the amount of Rh(III) adsorbed per unit mass of the resin at equilibrium and time t (h), respectively, and k_1 (1/h) and k_2 (g/mgh) the rate constants of the pseudo-first-order and pseudo-second-order adsorption, respectively.

It is observed that the pseudo-first-order model fits the experimental results with higher regression correlation coefficients R^2 values (0.9996–0.9997) than pseudo-second-order model (R^2 from 0.9632 to 0.9803) (Table 4). The higher R^2 values indicated that the
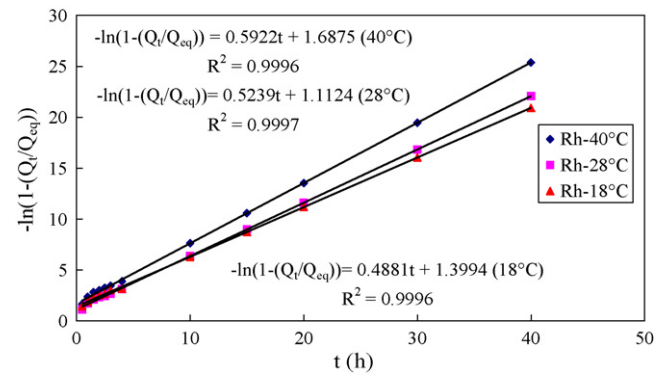

Fig. 6. Pseudo-first-order kinetics for Rh(III) adsorption on the resin at different temperatures (chloride solution = 60 mL; initial Rh(III) concentration = 8.9 ppm; resin = 0.5000 g; 150 rpm; 40 h).

adsorption kinetics data are better represented by the pseudo-first-order model.

The rate constants k_1 and k_2 were calculated from the slopes of the linear plots of $\ln(1 - (Q_t/Q_{eq}))$ and $1/(1 - (Q_t/Q_{eq}))$ versus time t, respectively (Figs. 6 and 7) and listed in Table 4. The Q_{eq} values measured by experiments at equilibrium time 40 h were 0.48, 0.45 and 0.40 mg/g for temperatures 18, 28 and 40 °C, respectively. The adsorption rate constant k_1 were 0.49, 0.52 and 0.59 h^{-1} for temperatures 18, 28 and 40 °C, respectively (Table 4). Obviously, the higher the temperature, the larger the adsorption rate constant. The linear plot of $\ln k_1$ versus $(10^3/T)$ (K^{-1}) (Fig. 8(a)) with regression correlation coefficient 0.9496 indicated the applicability of the following Arrhenius Eq. (14).

$$\ln k_1 = \ln A - \frac{E_{a,1}}{RT} \tag{14}$$

where A is the pre-exponential factor, $E_{a,1}$ the apparent adsorption activation energy (J/mol), R the gas constant (8.314 J K^{-1} mol^{-1}), and T the temperature (K). The apparent adsorption activation energy $E_{a,1}$ for the pseudo-first-order was calculated from the slope of the linear plot of $\ln k_1$ versus $(10^3/T)$ and found to be 6.54 J/mol. The adsorption rate constant k_2 were 11.77, 11.52 and 29.79 (g/mgh) for temperatures 18, 28 and 40 °C, respectively. The linear plot of $\ln k_2$ versus $(10^3/T)$ (K^{-1}) (Fig. 8(b)) with regression correlation coefficient 0.66 indicated the poor applicability of the following Arrhenius Eq. (15).

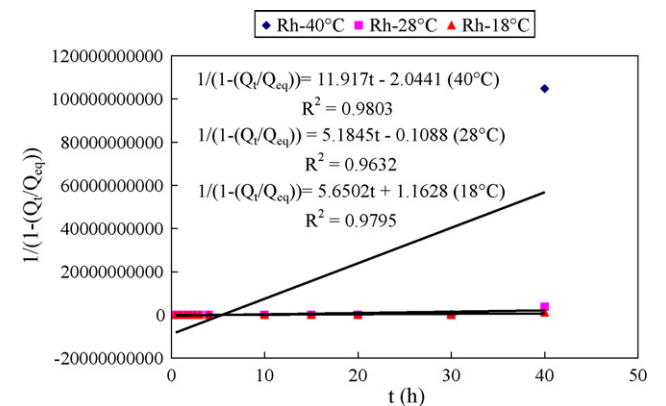$$\ln k_2 = \ln A - \frac{E_{a,2}}{RT} \tag{15}$$

Fig. 7. Pseudo-second-order kinetics for Rh(III) adsorption on the resin at different temperatures (chloride solution = 60 mL; initial Rh(III) concentration = 8.9 ppm; resin = 0.5000 g; 150 rpm; 40 h).
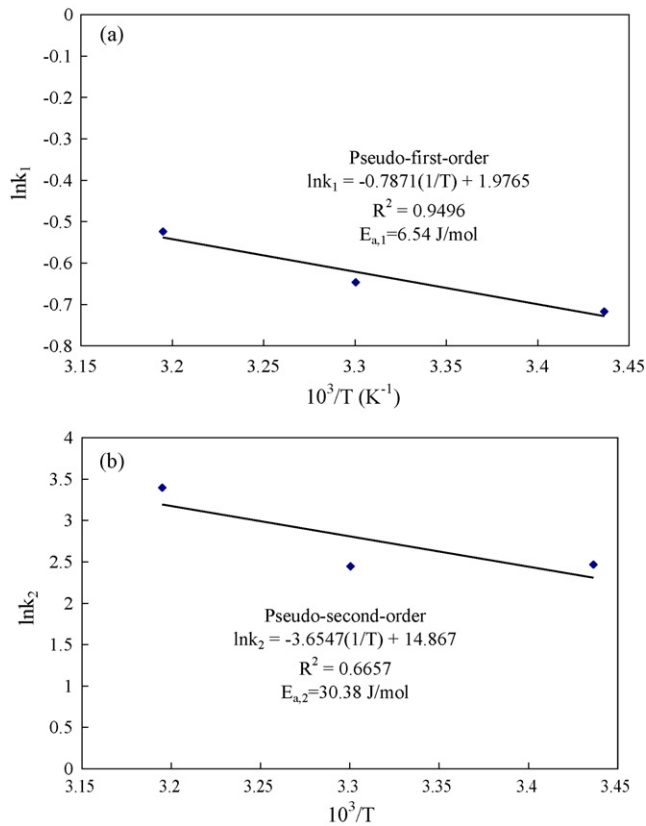
Fig. 8. (a) Arrhenius equation plot for Rh(III) pseudo-first-order adsorption on resin Diaion WA21J (chloride solution = 60 mL; initial Rh(III) concentration = 8.9 ppm; resin = 0.5000 g; 150 rpm; 40 h) (b) Arrhenius equation plot for Rh(III) pseudo-second-order adsorption on resin Diaion WA21J (chloride solution = 60 mL; initial Rh(III) concentration = 8.9 ppm; resin = 0.5000 g; 150 rpm; 40 h).

The apparent adsorption activation energy $E_{a,2}$ for the pseudo-second-order was calculated from the slope of the linear plot of $\ln k_2$ versus $(10^3/T)$ and found to be 30.38 J/mol. According to the regression correlation coefficients R^2 of pseudo-first-order and pseudo-second-order Eqs. (10) and (13), respectively, as well as the regression correlation coefficients R^2 of Eqs. (14) and (15), respectively, it was concluded that the experimental data of kinetics obtained in this work could be better simulated by pseudo-first-order kinetic model.

3.4.2. External diffusion model

At early times of contact (between 0 and 20 min of contact, for example) the system could be simplified by assuming that the concentration of Rh(III) on the resin surface tended toward zero (pure external diffusion) and the intraparticle diffusion to be negligible. Thus, Ficks' laws may be applied to describe mass-transfer rate of external diffusion. The diffusion flux J of Ficks' law could be expressed in Eq. (16).

$$J = k_f C_b = -\frac{dn_b}{Adt} = -\frac{VdC_b}{Adt} \tag{16}$$

where C_b is bulk concentration of Rh(III) (mol/m^3), k_f external mass-transfer coefficient of Rh(III) (m/h), A the resin exchange surface (m^2), V the volume of bulk solution (m^3) and t diffusion time (h).

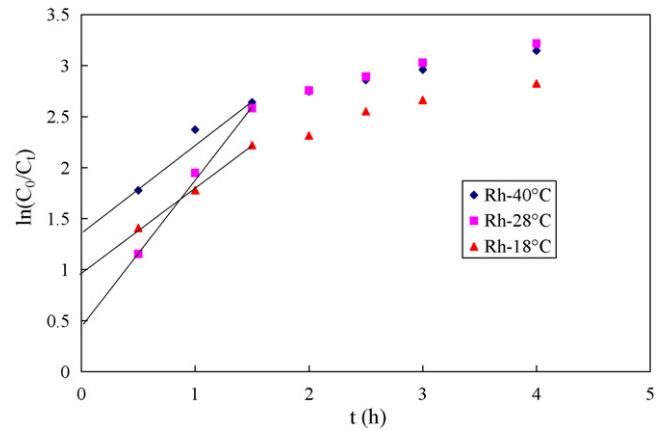$$-\int_0^t k_f \frac{A}{V} dt = \int_{C_0}^{C_t} d\ln C_b$$

Fig. 9. External diffusion model for Rh(III) adsorption on the resin at different temperatures (chloride solution = 60 mL; initial Rh(III) concentration = 8.9 ppm; resin = 0.5000 g; 150 rpm; 40 h).

$$\ln \frac{C_0}{C_t} = k_f \frac{A}{V} t \tag{17}$$

where C_0 and C_t are the bulk concentrations of Rh(III) (mol/m^3) at time of 0 and t, respectively. If external diffusion was a rate-controlling step at the beginning of Rh(III) adsorption process, there was a linear relationship between $\ln C_0/C_t$ and t as described by Eq. (17) at a certain temperature. However, such linear relationships did not exist for the three temperatures at the time range between 0 to several hours (Fig. 9). Although there were quasi-linear relationships between $\ln C_0/C_t$ and t between 0.5 to 1.5 h (Fig. 9), the lines did not pass through the original. Thus external diffusion was not rate-controlling step after 0.5 h.

3.4.3. Intraparticle diffusion model

Besides for adsorption on the external surface of adsorbent, there is also a possibility of transport of adsorbate Rh(III) ions from the external surface to the internal pores of the adsorbent resin (intraparticle diffusion). The most commonly used technique for identifying the mechanism involved in the adsorption process is by using intraparticle diffusion model [15] given by Eq. (16):

$$Q_t = k_{id} t^{1/2} + c \tag{18}$$

where Q_t (mg/g) is the amount of Rh(III) adsorbed per unit mass of the resin at time t (h), k_{id} the intraparticle diffusion rate constant (mg g^{-1} h$^{-1/2}$), and c is the intercept. For the intercept c, McKay et al. [16] have indicated that "extrapolation of the linear portion of the plot back to the y axis provides intercepts which are proportional to the extent of the boundary layer thickness, that is, the larger the intercept the greater the boundary layer effect".

Plots of Q_t versus $t^{1/2}$ for the three temperatures are shown in Fig. 10. From the figure it is observed that there are three linear regions. The first linear portion depicts diffusion in large pores, the second the diffusion in small pores and the third equilibrium. The size ranges of the large pores or the small pores were not clear. The intraparticle diffusion rate constants, $k_{id,1}$ and $k_{id,2}$, corresponding for the diffusion in large and small pores, respectively, are determined from the slopes of the linear regions while the intercepts, c_1 and c_2 are proportional to the boundary layer thickness. The values of these rate constants and intercepts are listed in Table 4. The values of intercept, c_1, were about 0.27, 0.17 and 0.25 mg/g, for temperatures 18, 28 and 40 °C, respectively, which indicates that the thickness of the boundary layer became the thinnest at 28 °C, that is, the external diffusion resistance was the smallest at 28 °C. According to the intercepts c_1 of the three temperatures (Table 4), the boundary layer diffusion (external diffusion)
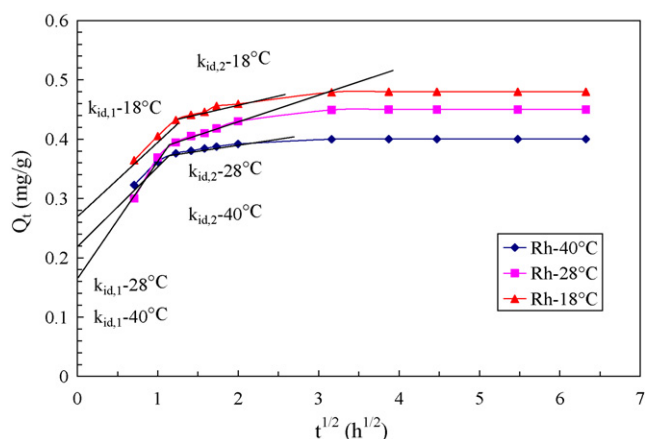
Fig. 10. Intraparticle diffusion model for Rh(III) adsorption on the resin at different temperatures (chloride solution = 60 mL; initial Rh(III) concentration = 8.9 ppm; resin = 0.5000 g; 150 rpm; 40 h).

was apparent. The external diffusion was completed within 0.5 h ($t^{1/2} = 0.7 \, h^{1/2}$) and the stages of intraparticle diffusion control (linear portions) were then attained. The diffusion control in large pores was demonstrated between 0.5 and 1.5 h ($t^{1/2} = 0.7$–$1.2 \, h^{1/2}$). Then the diffusion control in small pores was displayed between 1.5 and 10 h ($t^{1/2} = 1.2$–$3.2 \, h^{1/2}$). The values of $k_{id,1}$ for the three temperatures 18, 28 and 40 °C were 0.13, 0.18 and 0.10 mg g^{-1} h$^{-1/2}$ respectively, which imply that the biggest rate of large pore diffusion was reached at 28 °C. The ratio of $k_{id,1}/k_{id,2}$ was about 4 for each temperature. Thus, the diffusion rate in large pores is much faster than that in small pores. Obviously, the stage of diffusion control in large pores was much shorter than that in small pores, which could be attributed to faster diffusion rate of Rh(III) in large pores. In general, the adsorption rate of Rh(III) was controlled by external diffusion before 0.5 h, then by the diffusion in large pores between 0.5 and 1.5 h, followed by the diffusion in small pores between 1.5 and 10 h. After 10 h, the adsorption equilibrium was reached. Thus, the adsorption rate of Rh(III) was controlled by intraparticle diffusion in most of time.

3.5. Nitrogen adsorption/desorption measurements

Surface area measurements were conducted according to the Brunauer–Emmett–Teller (BET) gas (nitrogen) adsorption method. Adsorption/desorption isotherms for both the original and used solid resins are shown in Fig. 11(a). Multipoint BET analysis of multiple adsorption isotherms yields a BET specific surface area of 33 m^2/g and a total pore volume of 0.052 mL/g for the original resin and corresponding 27 m^2/g and 0.518 mL/g for the used resin. After adsorption, the surface areas of the resin decreased by 18% while the total pore volume increased by 90%.

Determination of the pore diameter distribution based on the nitrogen desorption isotherm used the Barret–Joyner–Halenda model. Pore diameter distributions for both the original and used resins are shown in Fig. 11(b). Based on the figure, the calculated mean pore diameters (d) for the original and used resins were 63 Å (mesoporous region) and 756 Å (macroporous region), respectively. After adsorption, the mean pore diameter of the resin increased by 91%. This value was close to the increased percentage of total pore volume. For lg$d$ < 2.2 (d < 158 Å), there was no significant variation in pore distribution before and after adsorption. However, for the pores of the same diameter, the pore number at the diameter range of 2.44 < lg$d$ < 3.23 (275 Å < d < 1698 Å) decreased significantly after adsorption. In the mean time, for lg$d$ > 2.44 (d > 275 Å), pore number increased with increasing pore diameter for the used resin. Thus
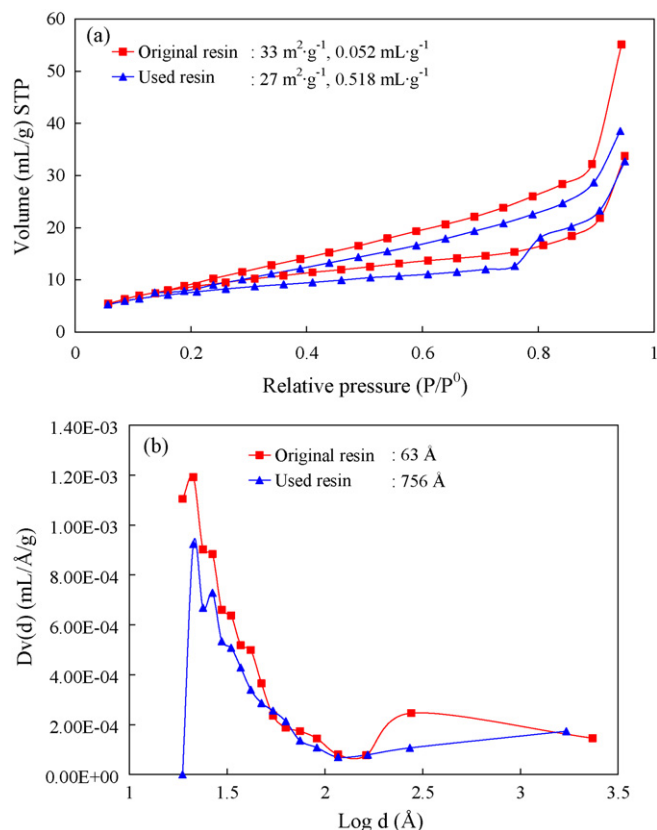

Fig. 11. Nitrogen adsorption measurements of the resins: (a) nitrogen adsorption/desorption isotherms of original and used resins (squares and triangles, respectively). The average BET specific surface areas of original and used resins were 33 and 27 m^2/g, respectively. The total pore volumes of original and used resins were 0.052 and 0.518 mL/g, respectively. (b) BJH desorption pore size distributions of original and used resins (squares and triangles, respectively). The average pore diameters of original and used resins were 63 and 756 Å, respectively.

it is reasonable to speculate that the pores at the diameter range 2.44 < lg$d$ < 3.23 (275 Å < d < 1698 Å) were converted to larger pores during the adsorption, which resulted in a remarkable increase in the mean pore diameter and total pore volume.

The resin Diaion W21J is a weakly basic anionic exchanger. There are basic organic functional groups on the surface of the resin. Probably the 10% (w/w) hydrochloric acid contained in the chloride solution reacted with part of these organic bases and resulted in the formation of more macropores. Rhodium chlorides mainly existed in the form of macro-molecule Rh(H$_2$O)$_2$Cl$_4$$^-$ under the present conditions (3.3 M HCl). More resistance was met when it diffused in small pores. Probably because of the step-wise increasing number of macropores of the resin during the adsorption, it was observed in this work that anion Rh(H$_2$O)$_2$Cl$_4$$^-$ could be adsorbed on such kind of anionic macropore resin. It was found by us in other experiments that many common commercial micro- or meso pore anionic resin, cationic resins and some activated carbons could not adsorb Rh(III) at all, although some of them demonstrated excellent adsorption for Pt and Pd ions in the chloride solution (not shown). In addition to Rh, Pd and Pt, other metal ions such as Al, Fe, Si, Zn and Pb were also adsorbed on the resin. The adsorption of metal ions inside the pores of the resin probably resulted in the decrease of specific surface area of the resin (Fig. 10(a)).

4. Conclusions

Thermodynamic and kinetics studies for adsorption of Pd(II) complexes from the chloride solutions on anionic exchange resin

Diaion WA21J were carried out. The following conclusions can be drawn.

(1) The adsorption efficiencies of Rh, Pd, Pt, Al, Fe, Si, Zn and Pb were 89.89%, 90.58%, 91.53%, 0.69%, 0.63%, 9.98%, 17.58% and 55.14%, respectively, and the adsorptions of Mn, Ca, Mg, Ni, Cu, La and Ba on the resin were negligible under the adsorption conditions.
(2) The adsorption equilibrium times for Rh(III) on the resin were about 10 h at 18, 28 and 40 °C under the adsorption conditions.
(3) The distribution coefficients (K_d) of Rh(III) decreased with the increase in initial Rh(III) concentration or in adsorption temperature.
(4) The isothermal adsorption of Rh(III) was found to fit Freundlich, Langmuir and Dubinin–Kaganer–Radushkevich models under the adsorption conditions. The adsorption of Rh(III) on the resin was favorable according to the values of $1/n$ and R_L from Freundlich and Langmuir adsorption isotherms, respectively. The maximum monolayer adsorption capacities Q_{max} and X_m of Rh(III) on the resin based on Langmuir and Dubinin–Kaganer–Radushkevich adsorption isotherms were 6.39, 6.61 and 5.81 mg/g as well as 12.15, 12.00 and 10.46 mg/g for temperatures 18, 28 and 40 °C, respectively. The apparent adsorption energy (E_{ad}) based on Dubinin–Kaganer–Radushkevich isotherm were −7.62, −7.45 and −7.96 kJ/mol for the temperatures 18, 28 and 40 °C, respectively. Rh(III) adsorption on the resin was basically a physical type, but very close to an ion-exchange type. So the resin can be used as a potential source for adsorption of Rh(III) from the chloride solution.
(5) The experimental data of kinetics obtained in this work could be better simulated by pseudo-first-order kinetic model and the apparent adsorption activation energy $E_{a,1}$ was 6.5 J/mol. The intraparticle diffusion was predominant in the whole adsorption process.
(6) After adsorption, both the mean pore diameter and total pore volume of the original resin increased by 90% while the BET specific surface area of the resin decreased by 18%. The formation of macropores during the adsorption probably explained why macro-molecule $Rh(H_2O)_2Cl_4^-$ could adsorb on such kind of anionic exchange resin.

Acknowledgements

References

[1] R. Gaita, S.J. Al-Bazi, An ion-exchanger method for selective separation of palladium, platinum and rhodium from solutions obtained by leaching automotive catalytic converters, Talanta 42 (1995) 249–255.
[2] C.H. Kim, S.I. Woo, S.H. Jeon, Recovery of platinum-group metals from recycled automotive catalytic converters by carbochlorination, Ind. Eng. Chem. Res. 39 (2000) 1185–1192.
[3] M. Benson, et al., The recovery mechanism of platinum group metals from catalytic converters in spent automotive exhaust systems, Resour. Conserv. Recycl. 31 (2000) 1–7.
[4] J.E. Hoffmann, Recovering platinum-group metals from auto catalysts, J. Met. 40 (6) (1988) 40–44.
[5] R.K. Mishra, A review of platinum group metals recovery from automotive catalytic converters, in: Precious Metals, IPMI, Allentown, PA, 1993, pp. 449.
[6] S.Y. Jin, Metal recovery and rejuvenation of metal-loaded spent catalysts, Catal. Today 44 (1998) 27–46.
[7] G. Levitin, G. Schmuckler, Solvent extraction of rhodium chloride from aqueous solutions and its separation from palladium and platinum, React. Funct. Polym. 54 (2003) 149–154.
[8] A. Mhask, P. Dhadke, Extraction separation studies of Rh, Pt and Pd using Cyanex 921 in toluene—a possible application to recovery from spent catalyst, Hydrometallurgy 61 (2001) 143–150.
[9] S. Basha, Z.V.P. Murthy, Kinetics and equilibrium models for biosorption of Cr(III) on chemically modified seaweed cystoseira indica, Process Biochem. 42 (11) (2007) 1521–1529.
[10] M.M. Saeed, et al., Investigation of the removal of lead by adsorption onto 1-(2-thiazolylazo)-2-naphthol (TAN) imbedded polyurethane foam from aqueous solution, J. Chin. Chem. Soc. 54 (2007) 173–183.
[11] S.H. Lin, R.S. Juang, Heavy metal removal from water by sorption using surfactant-modified montmorillonite, J. Hazard. Mater. B92 (2002) 315–326.
[12] C.C. Wang, L.C. Juang, C.K. Lee, T.C. Hsu, J.F. Lee, H.P. Chao, Effects of exchanged surfactant cations on the pore structure and adsorption characteristics of montmorillonite, J. Colloid Interface Sci. 280 (2004) 27–35.
[13] B.S. Krishna, D.S.R. Murty, B.S.J. Prakash, Thermodynamics of chromium(VI) anionic species sorption onto surfactant-modified montmorillonite clay, J. Colloid Interface Sci. 229 (2000) 230–236.
[14] W. Rudzinski, W. Plazinski, Studies of the kinetics of solute adsorption at solid/solution interfaces: on the possibility of distinguishing between the diffusional and the surface reaction kinetic models by studying the pseudo-first-order kinetics, J. Phys. Chem. C 111 (2007) 15100–15110.
[15] F.C. Wu, R.L. Tseng, R.S. Juang, Initial behavior of intraparticle diffusion model used in the description of adsorption kinetics, Chem. Eng. J. 153 (2009) 1–8.
[16] G. McKay, M.S. Otterburn, A.G. Sweeney, The removal of color from effluent using various adsorbents III silica: rate processes, Water Res. 14 (1980) 15–20.